The dynamics of the extratropical response to Madden-Julian Oscillation convection

Running Head: Dynamical Response to MJO

Katherine E. Lukens[1]
Department of Meteorology, The Pennsylvania State University, University Park, Pennsylvania

Steven B. Feldstein[2]
Department of Meteorology, The Pennsylvania State University, University Park, Pennsylvania

Changhyun Yoo
Department of Atmospheric Science and Engineering, Ewha Womans University, Seoul, South Korea

Sukyoung Lee
Department of Meteorology, The Pennsylvania State University, University Park, Pennsylvania
School of Earth and Environmental Sciences, Seoul National University, South Korea

[1]Current affiliation: Department of Atmospheric and Oceanic Science, University of Maryland, College Park, Maryland

[2]Corresponding author address: Steven Feldstein, Department of Meteorology, 516 Walker Building, The Pennsylvania State University, University Park, PA, 16802, USA.
Email: sbf1@meteo.psu.edu

Abstract

The Rossby wave source (RWS) and the corresponding extratropical wave response to tropical convection associated with different phases of the Madden-Julian Oscillation (MJO) is investigated with the dynamical core of a climate model. The initial flow is specified to correspond to the boreal winter climatological flow and an imposed tropical heating that is derived from the observed precipitation for all 8 MJO phases. One key question addressed here is why does the extratropical Rossby wave train depart the subtropics at a longitude well to the east of the RWS.

For all 8 MJO phases, it is found that the extratropical response over the North Pacific and North America is almost entirely due to the MJO convection over the western tropical Pacific. The RWS is excited within the first 24 hours after the model heating is turned on. For MJO phases 1-3 and 8, the RWS leads to the development of a cyclonic anomaly over southeast Asia via advection of the climatological absolute vorticity by the anomalous divergent wind in the subtropics and by horizontal convergence in the tropics. MJO phases 4-7 show opposite features. The resulting anomaly is then advected eastward by the climatological zonal wind toward the central Pacific, after which dispersion into the extratropics and the excitation of a Pacific/North American teleconnection pattern takes place.

Key Words: tropical-extratropical interaction, Rossby wave source, Madden-Julian Oscillation, teleconnections

1. Introduction

The Madden-Julian Oscillation (MJO) is the dominant mode of atmospheric intraseasonal variability within the tropics. The MJO is a planetary-scale phenomenon that incudes both convective and circulation components with a 30-60 day period (Madden and Julian 1971). The convective component of the MJO takes on a dipole spatial structure characterized by enhanced convection over the tropical Indian Ocean along with a reduction in convection over the tropical western Pacific Ocean, and vice versa. Many studies have shown that the MJO has a substantial impact on the extratropics through its excitation of poleward propagating Rossby waves (Weickmann et al. 1985; Higgins and Mo 1997; Matthews et al. 2004; L'Heureux and Higgins 2008; Seo and Son 2012; Yoo et al. 2012a,b). An active MJO has also been shown to influence the development of both the North Atlantic Oscillation (NAO) (Cassou 2008; Lin et al. 2009; Riddle et al. 2012) and Pacific/North American (PNA) teleconnection patterns (Mori and Watanabe 2008; Johnson and Feldstein 2010; Moore et al. 2010; Roundy et al. 2010; Franzke et al. 2011; Riddle et al. 2012) with lead times of one to four weeks. Seo et al. (2016) examined the

extratropical temperature response to the MJO, focusing on three regions where the MJO has a large impact. They observed warming over East Asia and North America, and cooling over Eastern Europe one to three weeks after enhanced MJO convection over the tropical Indian Ocean. They showed that the warming over East Asia arises primarily from adiabatic subsidence associated with an enhanced local Hadley circulation. In contrast, for North America and Eastern Europe, the temperature changes were found to arise from horizontal temperature advection associated with Rossby waves that were excited by the MJO. The above long lead times suggest that the MJO can be used as a basis for the improvement of medium-range weather forecasting (Vitart and Molteni 2010; Johnson et al. 2014). (See also http://www.cpc.ncep.noaa.gov, where the MJO is used for operational forecasts at week 3 and 4 lead times.)

One complication when trying to understand how tropical convection can excite Rossby waves that depart the tropics and propagate into midlatitudes is that the convection occurs within a broad region of tropical easterlies. Since the phase speed of quasi-stationary Rossby waves such as those associated with the MJO is greater than that of the background tropical easterlies, according to the linear theory of (rotational) Rossby wave dispersion, these Rossby waves cannot propagate meridionally and are thus trapped within the tropics. However, as shown by Sardeshmukh and Hoskins (1988), poleward propagating Rossby waves can still be excited by tropical convection if the divergent circulation induced by convection can advect absolute vorticity out of the tropics into the subtropical westerlies, or if this divergent circulation is

associated with strong subtropical divergence or convergence. Mathematically, the former can be expressed by $-\mathbf{v_d}\bullet\nabla\zeta_{abs}$, and the latter by $-\zeta_{abs}\nabla\bullet\mathbf{v_d}$ where $\mathbf{v_d}$ is the divergent wind and ζ_{abs} is the absolute vorticity. The sum of these two terms is commonly referred to as the Rossby wave source (RWS) (Sardeshmukh and Hoskins 1988). The vorticity anomaly generated by the RWS, in the presence of these westerlies, is then free to disperse poleward into higher latitudes. It is through this mechanism that it is usually thought that MJO convection excites Rossby waves that propagate into middle and high latitudes.

According to the RWS hypothesis, one might expect that poleward propagating Rossby wave trains would depart the subtropics from the longitude where the MJO-excited anomalies are first generated, that is, where the RWS associated with the MJO is a maximum. As we will see in this study, there are three regions in the Northern Hemisphere where the RWS associated with the MJO is a local maximum - over the Indian subcontinent, the eastern coast of China and the adjacent East China Sea, and southeast Asia, with the former two regions closely overlapping with the maximum climatological absolute vorticity gradient in the upper troposphere (Fig. 1). This would suggest that the poleward propagating Rossby wave trains associated with the MJO should depart the subtropics from eastern Asia. However, in the atmosphere, the poleward propagating Rossby wave train associated with the MJO departs the subtropics over the central Pacific and the extratropical response to the MJO occurs primarily over the North Pacific and North America. In other words, the longitude that the wave train leaves the subtropics differs from that where Rossby wave anomalies are first generated by the MJO. Furthermore, the

longitude that the wave train is observed to depart the subtropics corresponds to the jet exit region, where the climatological zonal wind is much weaker than that at the longitude of the maximum RWS. This suggests that the location of the jet exit region may play a crucial role in determining the longitude where the MJO-excited wave train departs the tropics. Based on geography proximity, this also suggests that perhaps the extratropical response to the MJO is being driven primarily by the MJO convection anomaly over the western Pacific and not that over the Indian Ocean.

Motivated by RWS theory, and also by apparent dissonance between the theoretical expectation and the observations, in this study, we address the following four questions: (1) What is the contribution of absolute vorticity advection by the divergent wind, i.e., $-\mathbf{v_d}\bullet\nabla\zeta_{\mathbf{abs}}$, and horizontal divergence $-\zeta_{\mathbf{abs}}\nabla\bullet\mathbf{v_d}$, to the RWS associated with the MJO? (2) Why is the MJO-linked North Pacific wave train located well to the east of the RWS? (3) Why does the Rossby wave train associated with the MJO depart the subtropics in the central Pacific? (4) What are the individual influences of the Indian Ocean and western Pacific Ocean convection on the extratropical response to the MJO?

In this study, to address these questions, we use the spectral dynamical core of a National Oceanic and Atmospheric Administration/Geophysical Fluid Dynamics Laboratory (NOAA/GFDL) climate model. Initial value calculations are performed with MJO-like tropical diabatic heating profiles, which are superimposed upon the Northern Hemisphere winter climatological flow. For addressing the questions raised above, there is a particular advantage to

using a model rather than analysing observational data to address the questions raised above. A problem with observational data is that there are secondary circulations induced by the ever-present extratropical synoptic-scale eddies. The secondary circulation, which maintains thermal wind balance, is characterized by a large horizontal divergence in the subtropics that makes a substantial contribution to the RWS. Thus, it can be challenging to disentangle the tropical convection contribution to the RWS from that associated with midlatitude synoptic-scale eddies. In the model, the initial flow does not include synoptic-scale eddies, i,e., there is no synoptic-scale eddy-driven secondary circulation at the beginning of the model integration. Furthermore, as shown in Jin and Hoskins (1995), for the type of model integration performed in this study, the generation of synoptic-scale eddies by baroclinic instability isn't fully complete until almost 3 weeks into the model integration. Therefore, since our model integrations will terminate after 9 days, a synoptic-scale eddy-driven secondary circulation remains unimportant throughout the model integration, which allows us to isolate the impact of MJO tropical convection on the extratropical circulation.

To investigate how the RWS develops in response to the model's tropical convective heating, we will examine the RWS every six hours within the first day of the model integration. This is because, as we will see, the RWS is established within 12-18 hours after the convective heating is turned on, and the excitement of Rossby waves is first apparent after 24 hours. In other words, the step-by-step sequence by which tropical convective heating excites the RWS and then Rossby waves, occurs very rapidly, within one day. Therefore, to understand the dynamics of the

causal relationship between MJO tropical convection, the RWS, and the generation of Rossby waves, it is critical to examine the detailed flow evolution during the first day of the model integration. To the best of our knowledge, such an examination of the initial evolution has not yet been performed. Previous studies examined the RWS either after several days in a model run or from a statistically steady state in either a model run or with observational data.

In section 2, the model, experiments, and method are presented. This is followed by the results in section 3 and the conclusions in section 4.

2. Model experiments, and method

a) Model experiments

We employ the spectral dry-dynamical core of a NOAA/GFDL climate model (Held and Suarez 1994). This model numerically solves the primitive equations, and in our application, the model is integrated at a triangular 42 horizontal resolution with 19 vertical normalized pressure (sigma) levels. Newtonian cooling is applied only to the temperature deviation from the climatological state. Rayleigh friction is applied to the six lowest model levels ($\sigma > 0.7$), with the damping time set to one day at the surface and decreasing with height. This model includes fourth-order horizontal diffusion with a 0.1-day time scale at the smallest resolvable scale and vertical diffusion with a 1.0-day time scale. A more complete description about the model can be found in Held and Suarez (1994).

As discussed in the introduction, an initial value calculation is performed. The initial state for this calculation consists of a background flow that is computed by averaging the daily fields of the European Centre for Medium-Range Weather Forecasts (ECMWF) ERA-Interim reanalysis data set (Dee et al. 2011) for the months of December, January, and February (DJF) from 1979 to 2008. To ensure that the initial state in the model is balanced, forcing terms are added to the model equations. These forcing terms are obtained by integrating the model equations forward in time by one time step, as in Franzke et al. (2004). MJO-like heating profiles are then added to the initial state. (Details on the MJO-like heating are presented below.) Yoo et al. (2012a) and Goss and Feldstein (2015) also used the same modelling approach with the NOAA/GFDL spectral dynamical core to investigate the extratropical response to the MJO.

Eight separate model runs are performed, one for each of the eight MJO phases, which are defined by the values of the Real-Time Multivariate MJO index of Wheeler and Hendon (2004). This index is determined from a combined empirical orthogonal functions analysis of the tropical 200- and 850-hPa zonal wind, and outgoing longwave radiation. MJO phase 1 corresponds to enhanced convection in the Indian Ocean and reduced convection in the western tropical Pacific Ocean. MJO phase 5 shows opposite features and the remaining six phases have characteristics that are intermediate between phases 1 and 5. The determination of the heating fields for the MJO phases follow the same procedure as in Yoo et al. (2012a). Briefly, anomalous precipitation composites are obtained for the eight MJO phases using the NOAA‐Climate Prediction Center Merged Analysis of Precipitation (CMAP) (Xie and Arkin 1997) dataset. (In this study, all

anomalies refer to deviations from the observed climatology.) The horizontal structure of the model's heating field, H, is expressed as

$$H = \frac{\rho_w L P}{\rho_a c_p D} \ ,$$

where P is the composite precipitation anomaly, ρ_w the density of water, L the latent heat of vaporization, ρ_a the air density, c_p the specific heat capacity of dry air at constant pressure, and *D* the vertical depth of the heating. The horizontal structures of the total and anomalous heating fields are shown in Fig. 2 for MJO phases 1 and 5 (Yoo et al. 2012a). As can be seen, the anomalous heating fields take on a dipole structure, with one extremum located over the tropical Indian Ocean and the other over the western tropical Pacific Ocean. As in Yoo et al. (2012a), the heating is specified to gradually decline from the equator to 30 degrees latitude in both hemispheres, beyond which it is set to zero, and an analytical vertical structure is specified which has a single maximum value near 500 hPa (Fig. 2). The model integrations are performed for 9 days, since each MJO phase typically lasts between 5 and 10 days. Also, over this time period, the additional forcing term has limited impact on the flow evolution (Franzke et al. 2004). The heating is gradually turned on over a 24-hour time period to suppress the excitement of large amplitude gravity waves. In our presentation, the number of hours and days that are indicated correspond to the time period that has passed after the initial 24-hour spin-up time period.

b) Method

The variables examined in this study include the daily 200-hPa streamfunction, horizontal wind, divergence, and relative vorticity. These variables are calculated on the model's sigma surfaces and are then linearly interpolated onto the 200-hPa pressure surface. The key approach in this study is to analyse each term in the vorticity equation at 200 hPa (Feldstein 2002) which can be symbolically written in pressure coordinates as

$$\frac{\partial \zeta'}{\partial t} = \sum_{i=1}^{7} \xi_i + R,$$

where

$$\xi_1 = \underbrace{\left\{-\left(v'_{\mathrm{r}} \frac{1}{a}\frac{df}{d\theta}\right)\right\}}_{1.1} + \underbrace{\left\{-\left(v'_{\mathrm{d}} \frac{1}{a}\frac{df}{d\theta}\right)\right\}}_{1.2}$$

$$\xi_2 = \underbrace{\{-[\,\overline{\mathbf{v_r}}\,] \cdot \nabla\zeta'\}}_{2.1} + \underbrace{\{-\mathbf{v}'_{\mathbf{r}} \cdot \nabla[\,\overline{\zeta}\,]\}}_{2.2} + \underbrace{\{-[\,\overline{\mathbf{v}_{\boldsymbol{d}}}\,] \cdot \nabla\zeta'\}}_{2.3} + \underbrace{\{-\mathbf{v}'_{\boldsymbol{d}} \cdot \nabla[\,\overline{\zeta}\,]\}}_{2.4}$$

$$\xi_3 = \underbrace{\{-\overline{\mathbf{v}^*_{\mathbf{r}}} \cdot \nabla\zeta'\}}_{3.1} + \underbrace{\{-\mathbf{v}'_{\mathbf{r}} \cdot \nabla\overline{\zeta^*}\}}_{3.2} + \underbrace{\{-\overline{\mathbf{v}^*_{\mathbf{d}}} \cdot \nabla\zeta'\}}_{3.3} + \underbrace{\{-\mathbf{v}'_{\mathbf{d}} \cdot \nabla\overline{\zeta^*}\}}_{3.4}$$

$$\xi_4 = \underbrace{\{-(f + \overline{\zeta})\nabla \cdot \mathbf{v}'_{\mathbf{d}}\}}_{4.1} + \underbrace{\{-\zeta'\nabla \cdot \overline{\mathbf{v}_{\mathbf{d}}}\}}_{4.2}$$

$$\xi_5 = \underbrace{\{(-\mathbf{v}'_{\mathbf{r}} \cdot \nabla\zeta')'\}}_{5.1} + \underbrace{(\{-\nabla \cdot (\mathbf{v}'_{\mathbf{d}}\zeta')\}')}_{5.2}$$

$$\xi_6 = \left\{-\mathbf{k} \cdot \nabla \times \left(\omega' \frac{\partial \overline{\mathbf{v}}}{\partial \mathrm{p}}\right)\right\} + \left\{-\mathbf{k} \cdot \nabla \times \left(\overline{\omega}\frac{\partial \mathbf{v}'}{\partial \mathrm{p}}\right)\right\} + \left\{-\mathbf{k} \cdot \nabla \times \left(\omega' \frac{\partial \mathbf{v}'}{\partial \mathrm{p}}\right)\right\}$$

$$\xi_7 = \{-\upsilon\nabla^4\zeta'\}$$

In these equations, ¶ is the relative vorticity, **v** the horizontal wind vector, *v* the meridional wind component, É the vertical wind component, *a* the earth's radius, p the pressure, **k** the unit vector in the vertical direction, *f* the Coriolis parameter, Å the diffusivity, and R a residual. The subscripts 'r' and 'd' denote the rotational and divergent horizontal wind components, respectively. A prime indicates an anomaly in time (i.e., a deviation from the model's initial climatological state) and an overbar denotes the time mean of the respective variables. Square brackets indicate a zonal average, and an asterisk represents a deviation from the zonal average. For the remaining terms, standard definitions apply. The term $\frac{\partial\zeta\prime}{\partial t}$ is computed via centered finite differencing. The various contributions to each of the ξ_i are denoted as follows. For ξ_1, the first and second terms are referred as term 1.1 and term 1.2, respectively. For ξ_2, the four terms are designated as term 2.1 through term 2.4. The other ξ_i all follow the same format.

As stated in Feldstein (2002), ¾ corresponds to anomalous planetary vorticity advection, ¾ to the interaction between the anomaly and the zonal mean climatological flow, ¾ to the interaction between the anomaly and the zonally asymmetric climatological flow, ¾ to the divergence term, ¾ the relative vorticity advection by the transient eddies, and ¾ the tilting terms. The sum of terms 1.2, 2.3, 2.4, 3.3, 3.4, 4.1, 4.2, and 5.2 corresponds to the RWS, while

sum of terms 1.1, 2.1, 2.2, 3.1, 3.2, and 5.1 represents vorticity advection associated with the rotational wind.

In contrast to previous studies on the PNA that employ the streamfunction tendency equation (e.g., Feldstein 2002), we instead choose to use the vorticity equation. This is because the model calculations indicate that there is a large cancellation between the advection of the climatological relative vorticity by the anomalous rotational and divergent wind fields, i.e., terms 2.2 and 3.2 tend to cancel as well as terms 2.4 and 3.4, when the inverse Laplacian operator is applied. When this operator is not applied, the contribution by the rotational wind is dominant.

3. Model results

We first focus on MJO phase 1, and then compare the results with those for the seven other MJO phases.

a) MJO phase 1

For MJO phase 1, the streamfunction tendencies are shown every 6 hours for the first day and then every two days until day 9 (Figs. 3 and 4). During the first day, a dipole anomaly develops in the Northern Hemisphere tropics, with a negative anomaly centred near 110°E and a positive anomaly centred near 100°W (Fig. 3). The negative anomaly propagates eastward and strengthens over the next two days, followed by continued eastward propagation and then

poleward dispersion from the subtropical central Pacific at a longitude of about 150°E by day 7 (Fig. 4). (Although it would be more precise to refer to this longitude as the west-central Pacific, for the rest of this study, for brevity, we refer to this longitude as the central Pacific.) During the following two days (see day 9), the streamfunction tendency anomalies over the North Pacific and Alaska strengthen while the subtropical Pacific anomaly weakens. The resulting wave train exhibits features resembling the negative phase of the PNA, as negative anomalies are seen over the subtropical Pacific and northwestern North America, and a positive anomaly over the North Pacific. The PNA-like wave field at day 9 resembles the wave field found in other idealized modelling studies with MJO tropical heating (e.g., Matthews et al. 2004; Seo and Son 2012). The streamfunction tendency anomaly that developed in the tropics near 100°W during the first day strengthened and propagated eastward during the following two days, and then continued to propagate eastward with a similar amplitude over the following six days.

To address the questions raised in the introduction, we diagnose the response to the model's tropical convection with the vorticity equation, as described in section 2. We first focus on the RWS terms. A comparison of the magnitude of the RWS terms finds that four terms, i.e., terms 1.2, 2.4, 3.4, and 4.1, are much greater than terms 2.3, 3.3, 4.2 and 5.2 during the first day, i.e., the maximum value of the sum of the former four terms is about 8 times larger than that of the latter four terms. The sum of terms 1.2, 2.4, and 3.4 corresponds to advection of the climatological absolute vorticity by the anomalous divergent wind, i.e., the divergent wind excited by the anomalous MJO tropical convection, and term 4.1 corresponds to the anomalous

horizontal divergence also triggered by the MJO convection. It is to be expected that these terms dominate the RWS during the first day, as the divergent flow is first excited in response to the convection, while the remaining RWS terms, which involve the anomalous vorticity, develop later, as rotational wind and vorticity anomalies are triggered by the above four RWS terms. For the remainder of this study, we will limit our focus to these four RWS terms.

The advection of the climatological absolute vorticity by the anomalous divergent wind (the sum of terms 1.2, 2.4, 3.4) and the anomalous horizontal divergence (term 4.1) for the first day are shown in Figs. 5 and 6, respectively. (Note that the corresponding streamfunction and vorticity tendency anomalies in Figs. 3, 5 and 6 must be of opposite sign.) As can be seen (Fig. 5), over southeast Asia and the adjacent oceans, the advection of absolute vorticity by the anomalous divergent wind generates a large positive vorticity anomaly in the subtropics to the south of the Korean Peninsula, as well as weaker negative vorticity anomalies in the deep tropics over the eastern Indian, western and central Pacific Oceans and over the Gulf of Mexico, the Indian subcontinent and Arabian Sea.

One can understand why the advection of the climatological absolute vorticity by the anomalous divergent wind is dominated by a single positive anomaly by examining the spatial structure of the climatological absolute vorticity (Fig. 1), the model's prescribed tropical heating structure (Fig. 2), as well as the anomalous horizontal divergent wind field (Fig. 6). Figure 1 shows that the meridional gradient of the climatological absolute vorticity reaches its largest value to the south of the Korean Peninsula and Japan. In fact, the meridional gradient of the

climatological absolute vorticity reaches its Northern Hemispheric maximum value at this location. From Figs. 2 and 6, it can be seen that the negative heating anomaly in the western tropical Pacific excites equatorward anomalous divergent wind vectors that extend poleward to 30°N where the climatological absolute vorticity gradient reaches its maximum value (Fig. 1). As a result, the advection of the climatological absolute vorticity by the anomalous divergent wind is dominated by a single large positive anomaly in the subtropics. This result highlights the importance of suppressed rainfall, because for MJO phase 1, the extratropical response to the MJO appears to arise primarily in response to the reduction in western Pacific tropical convection. Also, over the Indian and western Pacific Oceans, at 24 hours into the model integration, the corresponding horizontal divergence shows a quadrupole pattern, with positive anomalies centred over the Philippines and the Indian subcontinent and negative anomalies to the south of the Korean Peninsula and over the northern Indian Ocean. This quadruple horizontal divergence pattern can be understood as arising in response to the positive heating anomaly over the tropical Indian Ocean and the negative heating anomaly discussed above. It is also seen that the positive horizontal divergence anomaly over southeast Asia and the western tropical Pacific is larger in magnitude than the corresponding negative anomaly over the northern Indian Ocean. This can be explained by noting that the negative heating is located about 10° farther northward where the climatological absolute vorticity is larger. By comparing Figs. 5 and 6, we see that the northern half of the negative streamfunction tendency anomaly centred near 110°E (Fig. 3) arises in response to the positive advection of absolute vorticity by the anomalous divergent wind

(the opposing anomalous horizontal divergence at this location is weaker) and the southern half of the same negative streamfunction tendency in response to anomalous horizontal convergence. This dominance of the advection of absolute vorticity by the divergent wind over the horizontal divergence in the subtropics matches the findings of Mori and Watanabe (2008) for the RWS associated with the MJO in observational data.

The vorticity advection associated with the rotational wind, i.e., the sum of terms 1.1, 2.1, 2.2, 3.1, and 3.2 is shown for the first day in Fig. 7. As can be seen, the sum of these terms is small compared to the RWS terms throughout the first day. As is discussed above, this is to be expected, since the rotational wind and vorticity develop in response to the RWS. Important features that can be seen to emerge in Fig. 7 at 18-24 hours into the model integration are positive anomalies at 140°E, 20°N and 90°E, 25°N, and a negative anomaly at 120°E, 25°N. This tripole pattern contributes toward the weakening and longitudinal broadening of the negative streamfunction tendency anomaly in Fig. 3.

The amplitude of the RWS remained larger than that of the vorticity advection associated with the rotational wind through to the end of day 2, but by day 3, the relative amplitude of these two quantities reversed. By comparing Fig. 4 and Fig. 8, the latter showing the vorticity advection associated with the rotational wind from day 3 to day 9, it can be seen that positive vorticity advection (the weak positive anomaly across the western and central Pacific centred between 20°N and 25°N at days 7 and 9) associated with the rotational wind accounts for the eastward propagation of the negative streamfunction tendency anomaly toward the central

Pacific. (It should be noted that at the southeastern end of the negative streamfunction tendency anomaly in Fig. 4, where the eastward propagation is most apparent, the amplitude of the streamfunction tendency anomaly is weaker than it is farther upstream. This is consistent with the weak positive vorticity advection at this location.) The zonally-elongated spatial structure of this positive vorticity advection anomaly is consistent with trapping by the strong subtropical jet (Hoskins and Ambrizzi 1993). It is the trapping feature of the climatological zonal wind that prevents the streamfunction tendency anomaly in the subtropics from being able to propagate poleward from the western subtropical Pacific, where the RWS is largest, into the extratropics. As the zonal wind over the central subtropical Pacific is much weaker than that over the western subtropical Pacific, over the central subtropical Pacific, the anomaly is no longer trapped. We interpret this flow feature as allowing for Rossby waves to disperse into the extratropics. Consistently, as can be seen over the day 7 to day 9 time interval, the vorticity advection associated with the rotational wind accounts for the poleward wave propagation from the central Pacific toward Alaska, i.e., for the negative PNA-like response to MJO phase 1, as discussed in the introduction.

We next examine two key terms that contribute to the vorticity advection associated with the background climatological rotational wind: the vorticity advection by the background climatological wind (the sum of terms 2.1 and 3.1) and stationary eddy advection (Feldstein 2003) (relative vorticity advection associated with the climatological stationary eddies, i.e., the sum of terms 3.1 and 3.2). The vorticity advection by the background wind is shown at days 3

and 5 and the stationary eddy advection is shown at days 5 and 7 (Fig. 9). For the vorticity advection by the background climatological wind, it is helpful to compare the location of the two negative streamfunction tendency anomalies near 30°N at days 3 and 5 in Fig. 4 (centred near 105°E and 140°E at day 3, and near 105°E and 150°E at day 5) with the corresponding positive vorticity advection anomalies in Fig. 9 (centered near 105°E and 155°E at day 3, and near 115°E and 160°E at day 5). It can be seen that the two vorticity advection anomalies are located between 0 and 15 degrees to the east of the two streamfunction tendency anomalies. This indicates that the vorticity advection by the climatological wind is both amplifying the streamfunction tendency anomalies, and contributing to the eastward propagation of these anomalies. These results show that the eastward advection of the negative streamfunction tendency anomaly from southeast Asia to the central tropical Pacific is due to vorticity advection by the climatological subtropical jet. Furthermore, we see that stationary eddy advection in the central subtropical Pacific accounts for further amplification of the positive streamfunction tendency anomaly in this region, as well as the negative streamfunction tendency anomaly farther to the north. This behaviour follows that described in Hoskins et al. (1983), where low-frequency (period greater than 10 days) anomalies are amplified in the jet exit region, where the zonal gradient of the climatological zonal wind is negative. This takes place because zonally-elongated low-frequency anomalies, such as those in Fig. 4, are isotropised by the stretching deformation field in this region. As shown in Hoskins et al. (1983), isotropisation of eddies results in an increase in eddy kinetic energy.

b) The other MJO phases

The streamfunction tendencies for MJO phases 3, 5 (see Fig. 2), and 7 are shown for days 1 through 9 in Fig. 10. As can be seen, the streamfunction tendencies for MJO phase 3 show a negative PNA-like pattern at days 7 and 9 that resembles the spatial pattern for MJO phase 1, with the wave train departing the subtropics from the central Pacific, but with a smaller amplitude and being displaced about 20° longitude to the east. The most striking difference between the streamfunction tendencies for MJO phases 1 and 3 is the absence of positive anomalies in the Western Hemisphere. Figure 10 also shows that the MJO phase 5 and 7 streamfunction tendencies closely resemble those for phases 1 and 3, respectively, but with the signs of the anomalies reversed. The extratropical responses for MJO phases 8 and 2 were found to resemble that for MJO phase 1, i.e., a negative PNA-like spatial pattern, with the former phase having a smaller amplitude and the latter phase showing a larger amplitude (not shown). The extratropical responses for MJO phases 4 and 6 were found to resemble those for MJO phases 8 and 2, respectively, with anomalies of the opposite sign (not shown).

The two dominant RWS terms, i.e., the advection of the climatological absolute vorticity by the anomalous divergent wind (the sum of terms 1.2, 2.4, and 3.4) and the anomalous horizontal divergence (term 4.1) are shown at 24 hours into the model integration in Fig. 11, for MJO phases 3, 5, and 7. For MJO phase 3 (Fig. 11a), over the subtropical northwest Pacific, the positive vorticity advection by the anomalous divergent wind has a smaller amplitude, is displaced about 20° eastward, and has a smaller zonal extent than that for MJO phase 1. This is

to be expected since the negative heating anomaly for MJO phase 3 is much weaker than that for phase 1, and it is located at a longitude well to the east of the maximum climatological absolute vorticity gradient (see the OLR anomaly in Fig. 8 of Wheeler and Hendon (2004)). For MJO phases 5 and 7 (Figs. 11b and 11c), similar RWS anomalies are found but with the anomalies being of opposite sign to those for MJO phases 1 and 3, respectively. For the anomalous horizontal divergence, for MJO phase 3 (Fig. 11d), as for MJO phase 1, this quantity also takes on a quadrupole structure over southeast Asia and the northwest subtropical Pacific. Most notably, the positive horizontal divergence anomaly is similar to that for MJO phase 1, and the corresponding negative anomaly is weaker. For MJO phases 5 and 7 (Figs. 11e and 11f), the horizontal divergence anomalies are also found to be of opposite sign to those for MJO phases 1 and 3, respectively. With regard to the remaining four MJO phases, both RWS terms for MJO phase 8 (2) exhibit anomalies with a similar spatial structure but with a slightly smaller (larger) amplitude than that for MJO phase 1 (not shown). MJO phases 4 and 6 RWS terms show similar features to those for MJO phases 8 and 2, respectively, but with anomalies of opposite sign (not shown).

The above findings indicate that the responses to the heating associated with the 8 MJO phases can be placed into two categories. The heating for MJO phases 1-3 and 8 excite a negative PNA-like pattern whose amplitude varies with MJO phase. Analogously, the heating for MJO phases 4-7 excites a positive PNA-like pattern, also with different amplitudes. Furthermore, the generation mechanisms for the extratropical responses to MJO phases 1-3 and 8

are essentially the same, i.e., the initial negative streamfunction tendency anomaly over southeast Asia is triggered by positive vorticity advection by the anomalous divergent wind in the subtropics and by horizontal convergence farther southward. For MJO phases 4-7, the generation mechanism is the same but with anomalies of opposite sign, i.e., negative vorticity advection in the subtropics and horizontal divergence farther southward. After the initial excitation of the streamfunction tendencies, for all 8 MJO phases, an examination of the vorticity advection associated with the rotational wind finds that all PNA-like patterns develop from eastward vorticity advection by the climatological background flow followed by downstream dispersion from the central subtropical Pacific (not shown), as was found for MJO phase 1.

4. Conclusions

The model results presented in this study suggest the following sequence for the response to the tropical heating (see the schematic diagram, which relates to MJO phase 5; Fig. 12). (1) The positive heating anomaly over the Warm Pool region generates a RWS (due to both advection of the climatological absolute vorticity by the anomalous divergent wind in the subtropics and by anomalous horizontal divergence in the tropics) which excites a vorticity anomaly over southeast Asia. (2) This anomaly is then advected eastward by the climatological subtropical jet from southeast Asia toward the jet exit region over the central subtropical Pacific. Both from the time that this anomaly is generated and during its subsequent eastward propagation this anomaly appears to be trapped by the strong subtropical jet. As a result, the anomaly cannot propagate

poleward from the region of the largest RWS. (3) Once the anomaly enters the jet exit region, where the climatological zonal wind is much weaker, the anomaly is no longer trapped and poleward Rossby wave propagation ensues. Furthermore, the anomaly can be isotropised and amplified via stationary eddy advection. This leads to the formation of a positive PNA-like pattern. In response to MJO phase 1 where convection is suppressed over the warm pool, the anomalies take on the opposite sign, and a negative PNA-like pattern emerges.

It was found that the essential development features shown in Fig. 12 also describe the excitation of negative PNA-like features for MJO phases 8, 2, and 3, and positive PNA-like features for MJO phases 4, 6, and 7. For MJO phases 8, 2, and 3, the RWS anomalies were of the same sign as those for MJO phase 1, and for MJO phases 4, 6, and 7, the RWS anomalies were of same sign as those for MJO phase 5. For MJO phases 8, 1, 2 and 3, this resulted in the generation of a negative streamfunction anomaly over southeast Asia which was followed by eastward propagation due to advection by the climatological subtropical jet, followed by dispersion from the central subtropical Pacific and the formation of a negative PNA-like pattern. All features were reversed for MJO phases 4 to 7, as a positive streamfunction anomaly was generated over southeast Asia, followed by eastward advection by the background subtropical jet and the excitation of a positive PNA-like pattern.

The results from this study may have implications for the extratropical response to the MJO during El Niño events, when the jet exit region is extended eastward, and for La Niña events when the jet exit region retracts westward. Since it was found that the Rossby wave train departs

the subtropics in the jet exit region, the results of our study allude to their being an eastward-displaced PNA during El Niño and a westward-displaced PNA during La Niña. Our results also allude to a relationship between the strength of the subtropical jet and the amplitude of the PNA response to the MJO. For example, a stronger and narrower subtropical jet than that for the climatological background state may result in an increase in the amplitude of the advection of the climatological absolute vorticity by the anomalous divergent wind relative to that for the anomalous horizontal divergence. This would likely result in a PNA response with a larger amplitude. A weaker subtropical jet may yield opposite features. These types of calculations are planned for in future research.

In the introduction, the question was raised as to what is the individual influence of MJO convection over the tropical Indian Ocean compared to that over the western tropical Pacific Ocean on the extratropical wave train. With observational data, Goss and Feldstein (2016) found that the response to MJO convective heating over the western Pacific is much stronger than that associated with the convective heating over the Indian Ocean. An examination of the RWS for MJO phase 1 shows that the RWS associated with the Indian Ocean MJO convective heating is much smaller than that associated with the western tropical Pacific MJO heating (Figs. 5 and 6). These differences can be understood by the climatological absolute vorticity gradient in the subtropics being much stronger at the longitude of the western tropical Pacific MJO heating (Fig. 1). For this reason, it appears that Indian Ocean MJO convection has a much smaller impact on the extratropical wave train than does MJO convection over the western tropical Pacific.

Acknowledgments. We would like to thank two anonymous reviewers for their helpful comments on this manuscript. This study is supported by National Science Foundation Grants AGS-1036858 and AGS-1401220, and by National Oceanic and Atmospheric Administration Grant NA14OAR4310190. CY is supported by the Basic Science Research Program through the National Research Foundation of Korea (NRF) funded by the Ministry of Science, ICT, and Future Planning (2016R1C1B2006310.

References

Cassou C. 2008. Intraseasonal interaction between the Madden–Julian Oscillation and the North Atlantic Oscillation. *Nature* **455**: 523-527.

Dee DP, and co-authors. 2011. The ERA-interrim reanalysis: configuration and performance of the data assimilation system. *Q. J. R. Meteorol. Soc.* **137**: 553-579.

Feldstein SB. 2002.Fundamental mechanisms of the growth and decay of the PNA teleconnection pattern. *Q. J. R. Meteorol. Soc.* **128**: 775-796.

Feldstein SB. 2003. The dynamics of NAO teleconnection pattern growth and decay. *Q. J. R. Meteorol. Soc.* **129**: 901-924.

Franzke C, Lee S, Feldstein SB. 2004. Is the North Atlantic Oscillation a breaking wave? *J. Atmos. Sci.* **61**: 145-160.

Franzke C, Feldstein SB, Lee S. 2011. Synoptic analysis of the Pacific–North American teleconnection pattern. *Q. J. R. Meteorol. Soc.* **137**: 329-346.

Goss M, Feldstein SB. 2015: The impact of the initial flow on the extratropical response to Madden Julian Oscillation convective heating. *Mon. Wea. Rev.*, **143**: 1104-1211.

Goss M, Feldstein SB. 2016. Why do similar patterns of tropical convection yield extratropical circulation anomalies of opposite sign? *J. Atmos. Sci.* in press.

Held IM, Suarez MJ. 1994. Aproposal for the intercomparison of the dynamical cores of atmospheric general circulation models. *Bull. Amer. Meteor. Soc.* **75**: 1825-1830.

Higgins RW, Mo KC. 1997. Persistent North Pacific circulation anomalies and the tropical intraseasonal oscillation. *J. Climate* **10**: 223-244.

Hoskins BJ, James IN, White GH. 1983. The shape, propagation and mean-flow interaction of large-scale weather systems. *J. Atmos. Sci.* **40**: 1595-1612.

Hoskins BJ, Ambrizzi T. 1993. Rossby wave propagation on a realistic longitudinally flow. *J. Atmos. Sci.* **67**: 1661-1671.

Jin F, Hoskins BJ. 1995. The direct response to tropical heating in a baroclinic atmosphere. *J. Atmos. Sci.* **52**: 307-319.

Johnson NC, Feldstein SB. 2010. The continuum of North Pacific sea level pressure patterns: intraseasonal, interannual, and interdecadal variability. *J. Climate* **23**: 851-867.

Johnson NC, Collins DC, Feldstein SB, L'Heureux ML, Riddle EE. 2014. Skillful wintertime North American temperature forecasts out to four weeks based on the state of ENSO and the MJO. *Wea. and Forecasting* **29**: 23-38.

L'Heureux ML, Higgins RW. 2008. Boreal winter links between the Madden–Julian oscillation and the Arctic Oscillation. *J. Climate* **21**: 3040-3050.

Lin H, Brunet G, Derome J. 2009. An Observed Connection between the North Atlantic Oscillation and the Madden–Julian Oscillation. *J. Climate* **22**: 364–380.

Madden RA, Julian PR. 1971. Detection of a 40–50 Day Oscillation in the Zonal Wind in the Tropical Pacific. *J. Atmos. Sci.* **28**: 702–708.

Matthews AJ, Hoskins BJ, Masutani M. 2004. The global response to tropical heating in the Madden–Julian oscillation during the northern winter. *Q. J. R. Meteorol. Soc.* **130**: 1911-2011.

Moore RW, Martius O, Spengler T. 2010. The modulation of the subtropical and extratropical atmosphere in the Pacific basin in response to the Madden–Julian Oscillation. *Mon. Wea. Rev.* **138**: 2761-2779.

Mori M, Watanabe M. 2008. The growth and triggering mechanisms of the PNA: A MJO-PNA coherence. *J. Met. Soc. Japan*. Ser. II **86**: 213-236.

Riddle EE, Stoner MB, Johnson NC, L'Heureux ML, Collins DC, Feldstein SB. 2012. The impact of the MJO on clusters of wintertime circulation anomalies over the North American region. *Clim. Dyn.*, doi 10.1007/s00382-012-1493-y.

Roundy PE, MacRitchie K, Asuma J, Melino T. 2010. Modulation of the global atmospheric circulation by combined activity in the Madden–Julian Oscillation and the El Niño–Southern Oscillation during boreal winter. *J. Climate* **23**: 4045-4059.

Sardeshmukh PD, Hoskins BJ. 1988. The generation of global rotational flow by steady idealized tropical divergence. *J. Atmos. Sci.* **45**: 1228-1251.

Seo K-H, Son S-W. 2012. The global atmospheric circula- tion response to tropical diabatic heating associated with the Madden–Julian oscillation during northern winter. *J. Atmos. Sci.* **69**: 79-96.

Seo K-H, Lee H-J, Frierson DMW. 2016: Unraveling the teleconnection mechanisms that induce wintertime temperature anomalies over the Northern Hemisphere continents in response to the MJO. *J. Atmos. Sci.* **73**: 3557-3571.

Vitart F, Molteni F. 2010. Simulation of the Madden–Julian oscillation and its teleconnections in the ECMWF forecast system. *Q. J. R. Meteorol. Soc.*, **136**: 842-855.

Weickmann KM, Lussky GR, Kutzbach JE. 1985. Intraseasonal (30–60 day) fluctuations of outgoing longwave radiation and 250mb streamfunction during northern winter. *Mon. Wea. Rev.* **113**: 941-961.

Wheeler MC, Hendon HH. 2004. An all-season real-time multivariate MJO index: Development of an index for monitoring and prediction. *Mon. Wea. Rev.* **132**: 1917-1932.

Xie P, Arkin PA. 1997. Global precipitation: A 17-year monthly analysis based on gauge observations, satellite estimates, and numerical model outputs. *Bull. Amer. Meteor. Soc.* **78**: 2539-2558.

Yoo C, Lee S, Feldstein SB. 2012a. Arctic response to an MJO-like tropical heating in an idealized GCM. *J. Atmos. Sci*. **69**: 2379-2393.

Yoo C, Lee S, Feldstein SB. 2012b. Mechanisms of extratropical surface air temperature change in response to the Madden-Julian Oscillation. *J. Climate* **25**: 5777-5790.

List of Figures

Figure 1: Climatological absolute vorticity. The contour interval is 1.0×10^{-5} s^{-1}.

Figure 2: Spatial pattern of tropical heating used in this study, which is based on composites of (top) anomalous and (bottom) total precipitation associated with MJO phases (left) 1 and (middle) 5. Contour intervals are (top) 0.5 and (bottom) 2 K and the zero contours are omitted. Light (dark) shading indicates positive (negative) values. (right) Vertical structure of the tropical heating profile. [Reprinted from Yoo et al. (2012) with permission from the American Meteorological Society.]

Figure 3: Streamfunction tendency every 6 hours for the first 24 hours for MJO phase 1. Panels (a), (b), (c), and (d) correspond to the first 6 hours, 12 hours, 18 hours, and 24 hours in the

integration, respectively. The contour interval for the first panel is 0.1 m^2 s^{-2}, with values exceeding -0.1 and 0.1 shaded. The contour interval for the remaining panels is 0.5 m^2 s^{-2}, with values exceeding -0.5 and 0.5 shaded.

Figure 4: Streamfunction tendency for MJO phase 1. Days 3, 5, 7, and 9 are shown in panels (a), (b), (c), and (d), respectively. The contour interval is 3.0 m^2 s^{-2}, with values exceeding -3.0 and 3.0 shaded.

Figure 5: Advection of the climatological absolute vorticity by the anomalous divergent wind (sum of terms 1.2, 2.4, and 3.4) every 6 hours for the first 24 hours for MJO phase 1. Panels (a), (b), (c), and (d) correspond to the first 6 hours, 12 hours, 18 hours, and 24 hours in the integration, respectively. The contour interval is 4.0×10^{-12} m^2 s^{-2}, with values exceeding -4.0×10^{-12} and 4.0×10^{-12} shaded.

Figure 6: Coloured contours show the anomalous horizontal divergence (term 4.1) overlaid with associated wind vectors every 6 hours for the first 24 hours for MJO phase 1. Panels (a), (b), (c), and (d) correspond to the first 6 hours, 12 hours, 18 hours, and 24 hours in the integration, respectively. Coloured contours have a contour interval of 2.0×10^{-12} m^2 s^{-2}, with values exceeding -2.0×10^{-12} and 2.0×10^{-12} shaded.

Figure 7: Vorticity advection associated with the rotational wind (sum of terms 1.1, 2.1, 2.2, 3.1, and 3.2) every 6 hours for the first 24 hours for MJO phase 1. Panels (a), (b), (c), and (d) correspond to the first 6 hours, 12 hours, 18 hours, and 24 hours in the integration, respectively.

The contour interval for the 6-hour panel is 0.2×10^{-12} m^2 s^{-2}, with values exceeding -0.2×10^{-12} and 0.2×10^{-12} shaded. The contour interval for the 12-hour panel is 1.0×10^{-12} m^2 s^{-2}, with values exceeding -1.0×10^{-12} and 1.0×10^{-12} shaded. The contour interval for the remaining panels is 2.0×10^{-12} m^2 s^{-2}, with values exceeding -2.0×10^{-12} and 2.0×10^{-12} shaded.

Figure 8: Vorticity advection associated with the rotational wind (sum of terms 1.1, 2.1, 2.2, 3.1, and 3.2) for MJO phase 1. Days 3, 5, 7, and 9 are shown in panels (a), (b), (c), and (d), respectively. The contour interval is 0.5×10^{-11} m^2 s^{-2}, with values exceeding -0.5×10^{-11} and 0.5×10^{-11} shaded. The -0.5×10^{-11} and 0.5×10^{-11} m^2 s^{-2} contour lines are drawn.

Figure 9: Left column shows the vorticity advection by the background wind (sum of terms 2.1 and 3.1) for MJO phase 1 on (a) Day 3 and (b) Day 5. Right column shows the stationary eddy advection (sum of terms 3.1 and 3.2) for MJO phase 1 on (c) Day 5 and (d) Day 7. The contour interval for all panels is 1.0×10^{-11} m^2 s^{-2}, with values exceeding -1.0×10^{-11} and 1.0×10^{-11} shaded.

Figure 10: Streamfunction tendency for (a) MJO phase 3, (b) MJO phase 5, and (c) MJO phase 7. The contour interval is 3.0 m^2 s^{-2}, with values exceeding -3.0 and 3.0 shaded. Each column shows days 1, 3, 5, 7, and 9 of the integration for each phase.

Figure 11: Left column shows the advection of the climatological absolute vorticity by the anomalous divergent wind (sum of terms 1.2, 2.4, and 3.4) at 24 hours for (a) MJO phase 3, (b) MJO phase 5, and (c) MJO phase 7. Right column shows the anomalous horizontal divergence

(term 4.1) as coloured contours and corresponding wind vectors at 24 hours for (d) MJO phase 3, (e) MJO phase 5, and (f) MJO phase 7. The contour interval for the left column is 4.0×10^{-12} m^2 s^{-2}, with values exceeding -4.0×10^{-12} and 4.0×10^{-12} shaded. The contour interval for the right column is 2.0×10^{-12} m^2 s^{-2}, with values exceeding -2.0×10^{-12} and 2.0×10^{-12} shaded.

Figure 12: A schematic diagram of the three-step process through which tropical convection excites poleward propagating Rossby waves. See the text for details. The thick red contour represents the initial vorticity anomaly generated by the Rossby wave source (RWS), the thick blue contour the vorticity anomaly at later steps, the arrow denotes the Pacific subtropical jet, and the thin contour corresponds to a contour of upper tropospheric geopotential height.

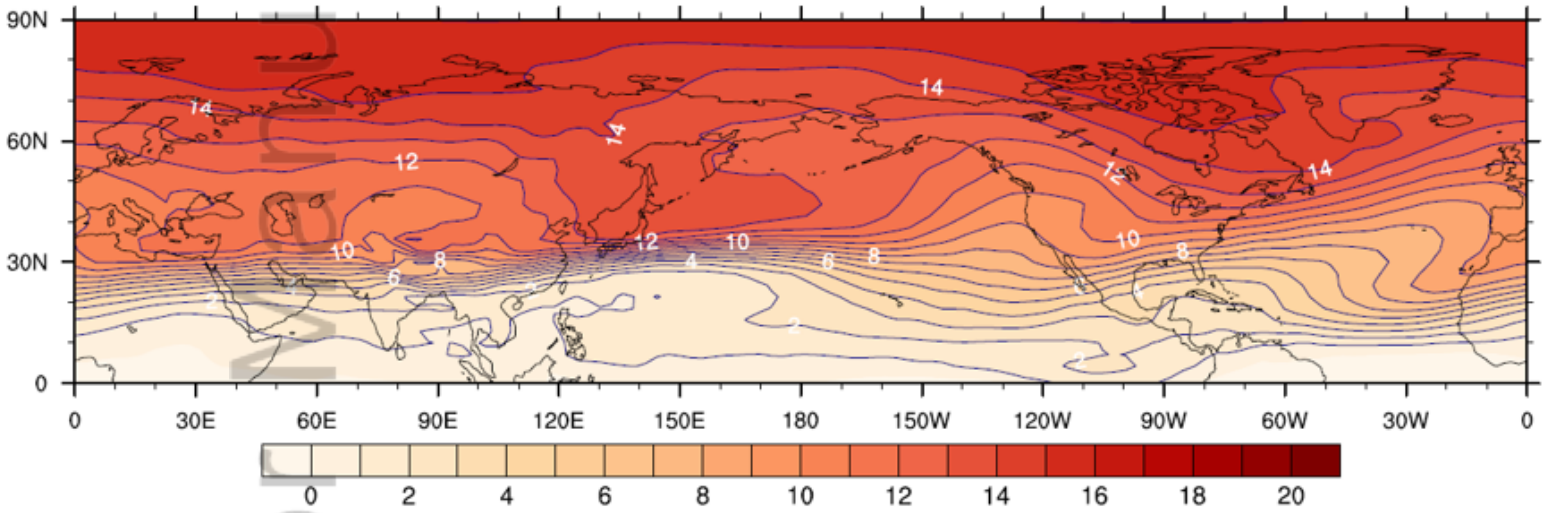

Lukens_et_al_QJRMS_Revised_Figure1.tif

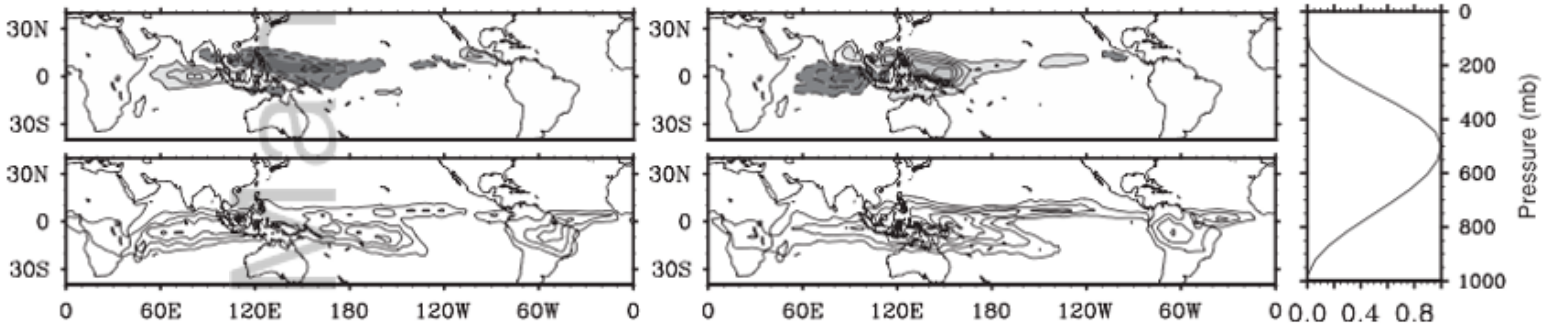

Lukens_et_al_QJRMS_Revised_Figure2.tif

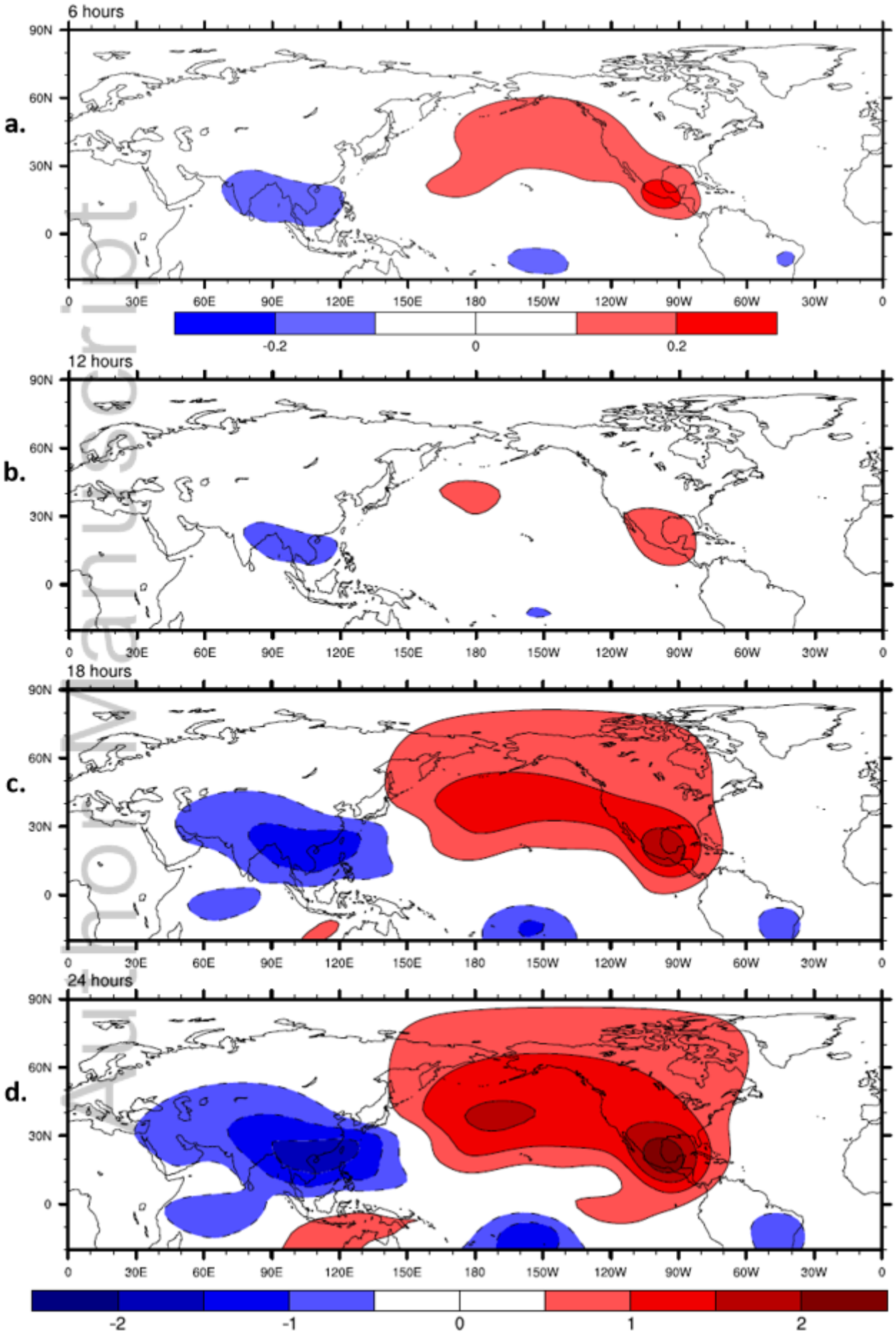

Lukens_et_al_QJRMS_Revised_Figure3.tif

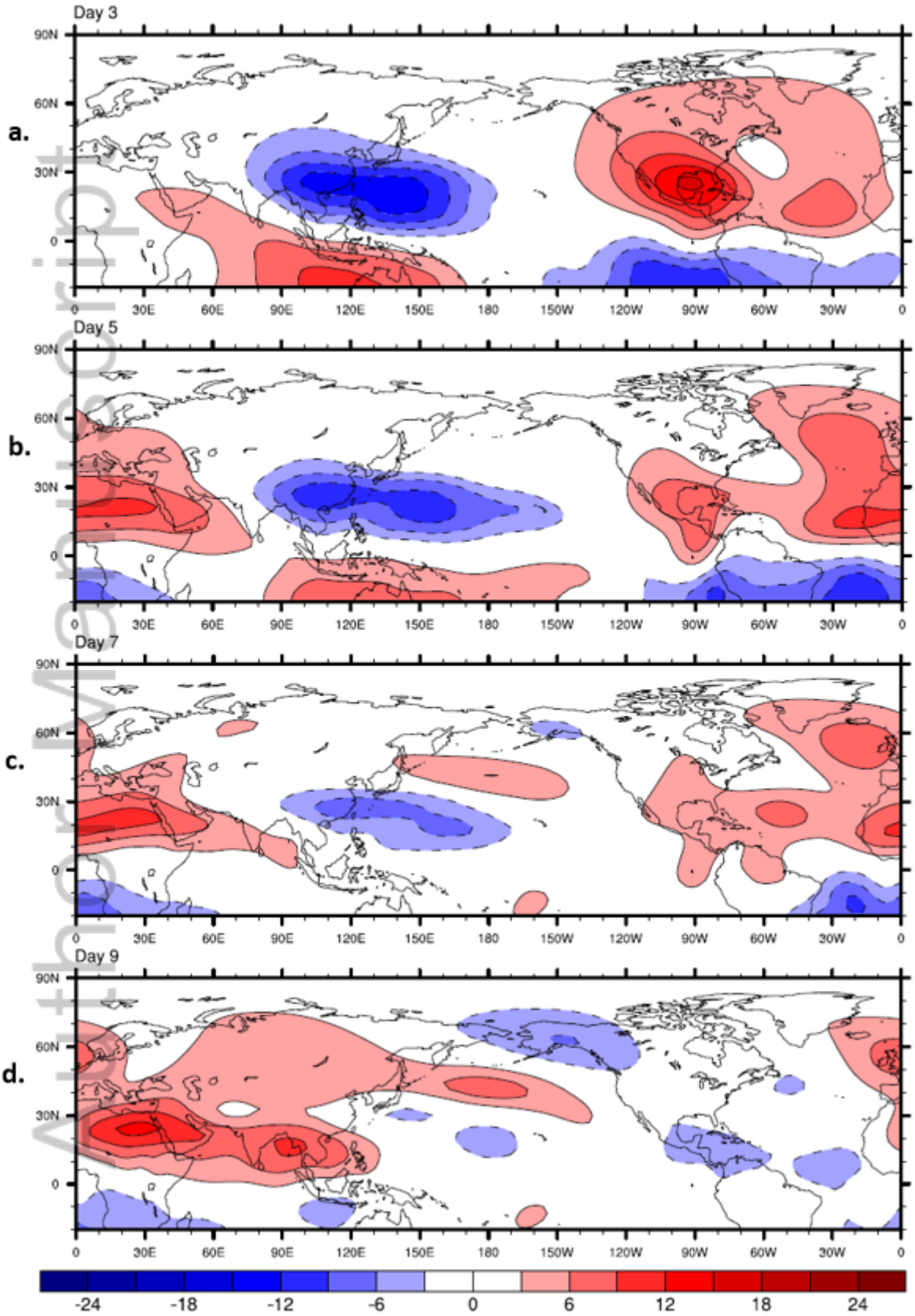

Lukens_et_al_QJRMS_Revised_Figure4.tif

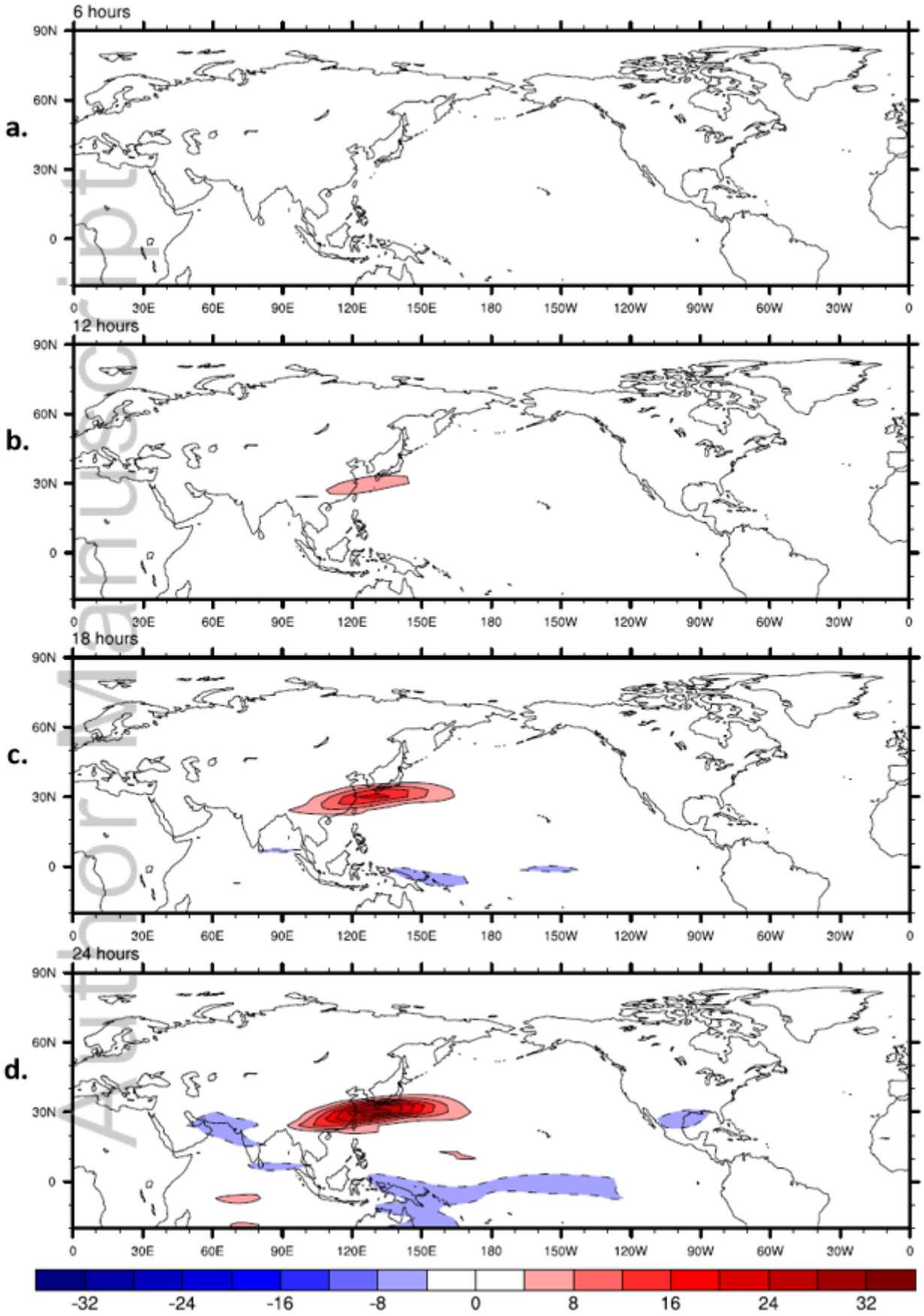

Lukens_et_al_QJRMS_Revised_Figure5.tif

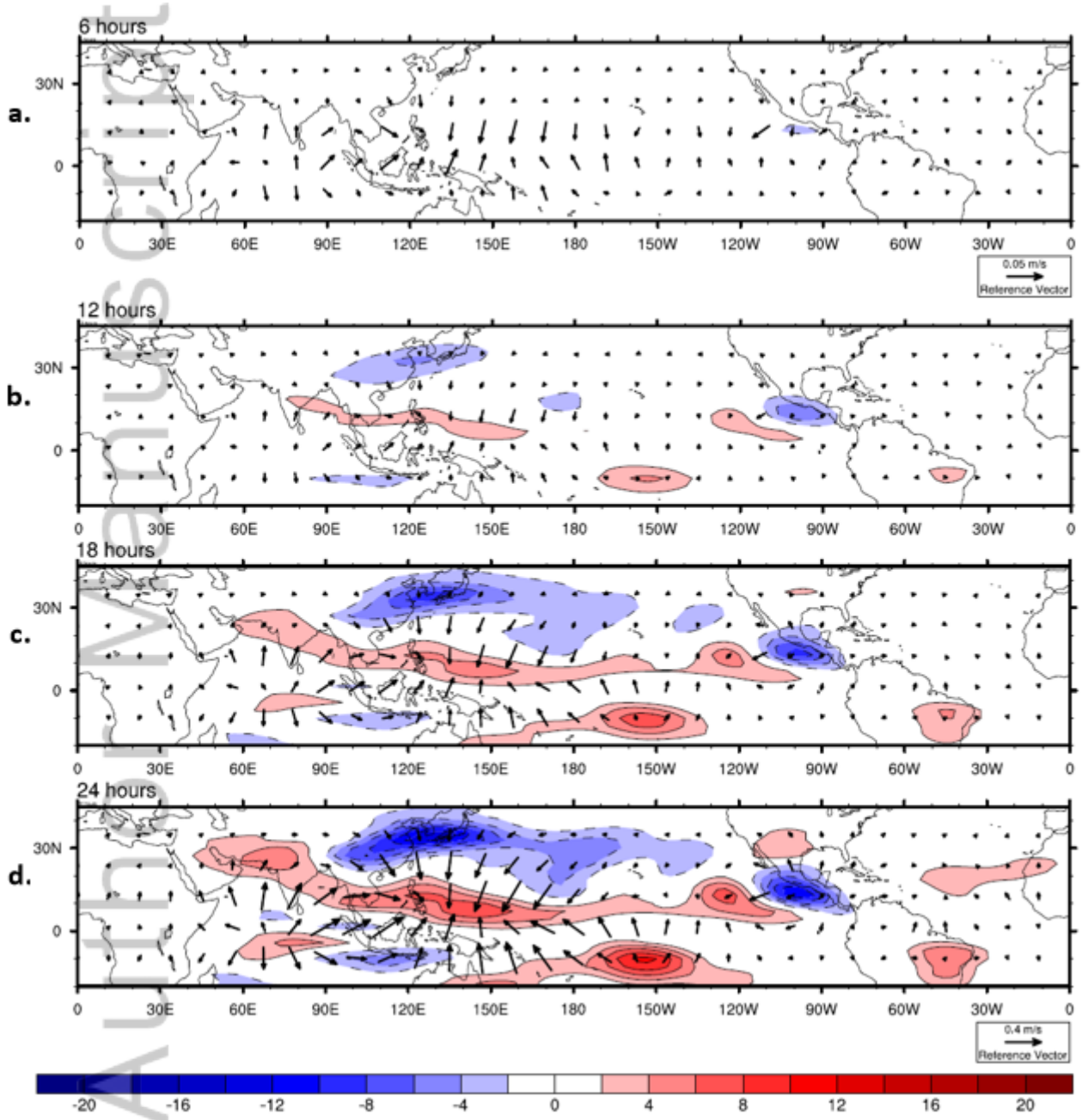

Lukens_et_al_QJRMS_Revised_Figure6.tif

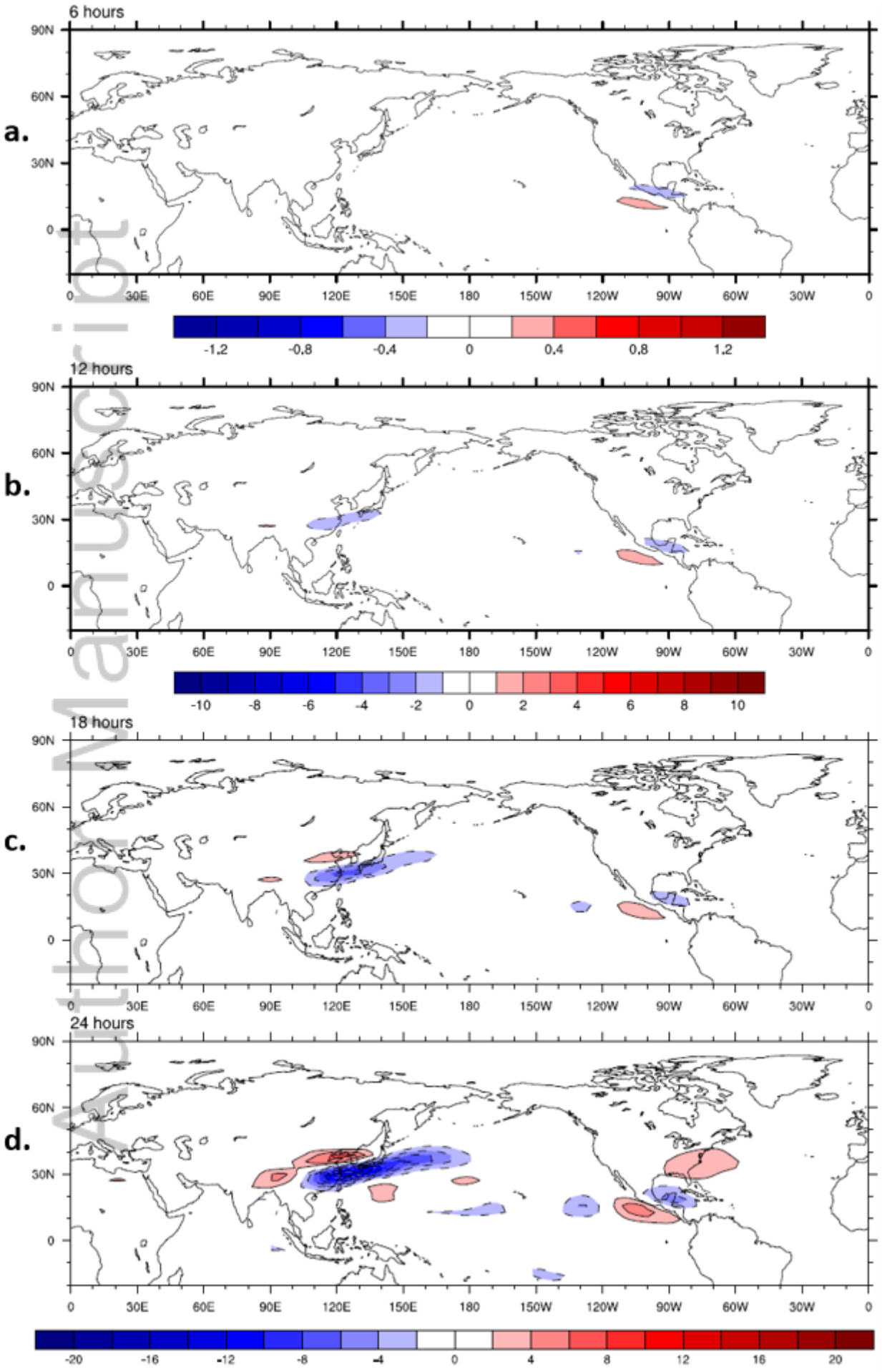

Lukens_et_al_QJRMS_Revised_Figure7.tif

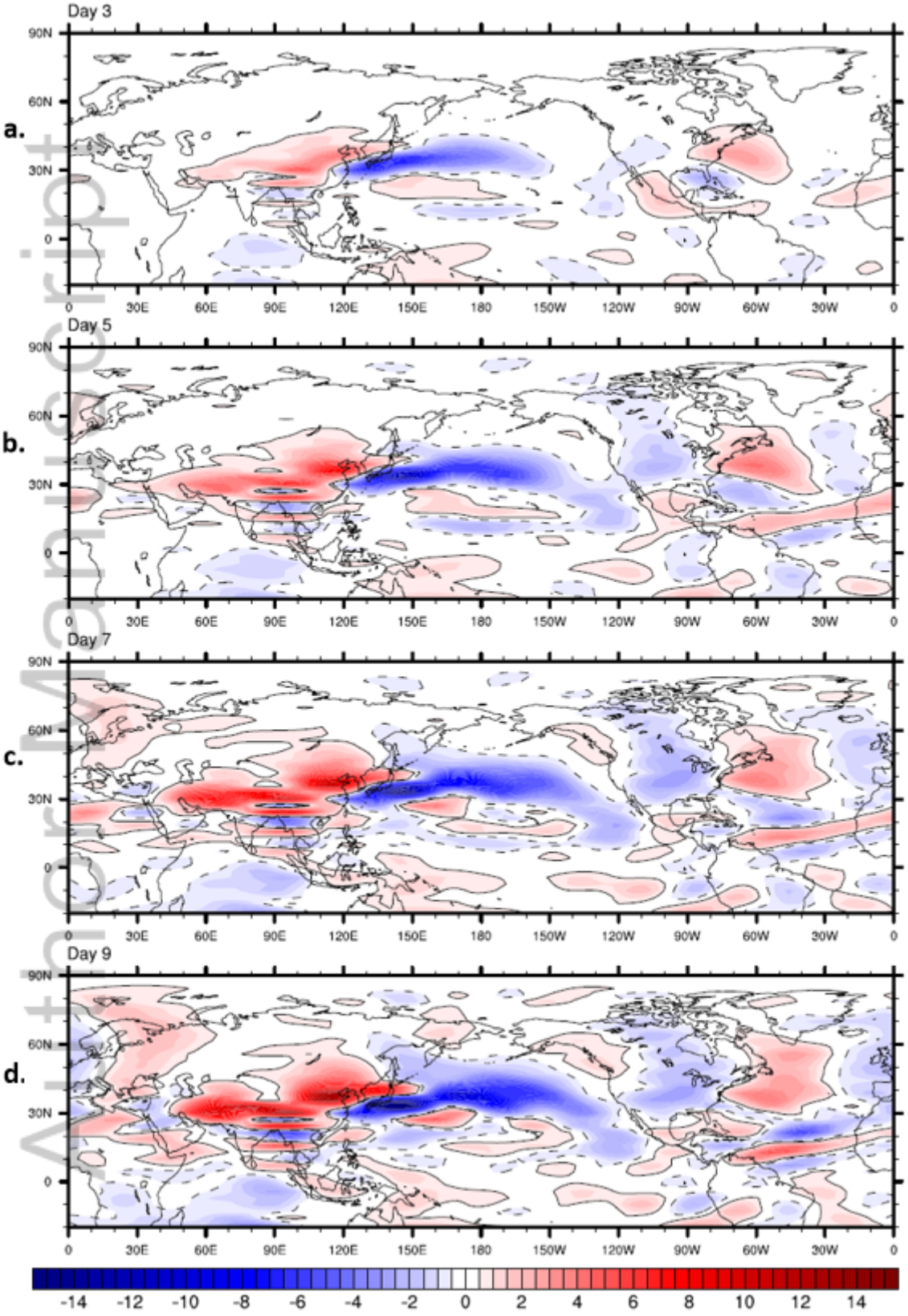

Lukens_et_al_QJRMS_Revised_Figure8.tif

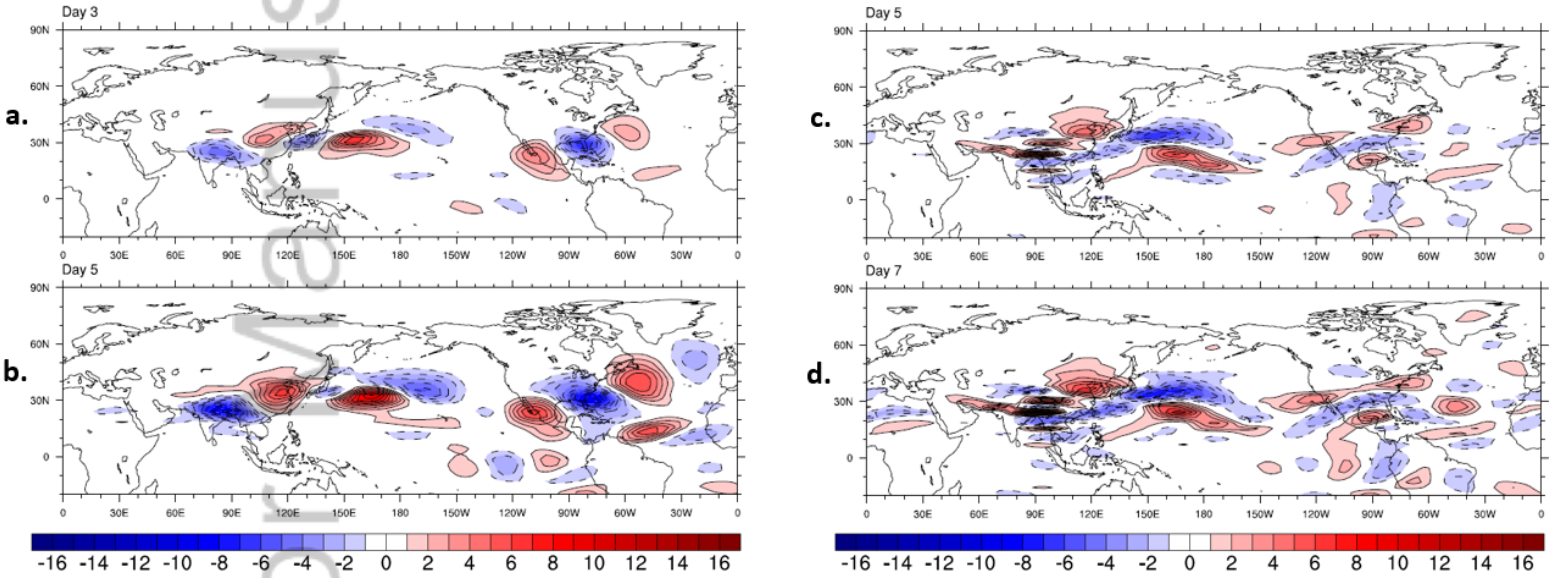

Lukens_et_al_QJRMS_Revised_Figure9.tif

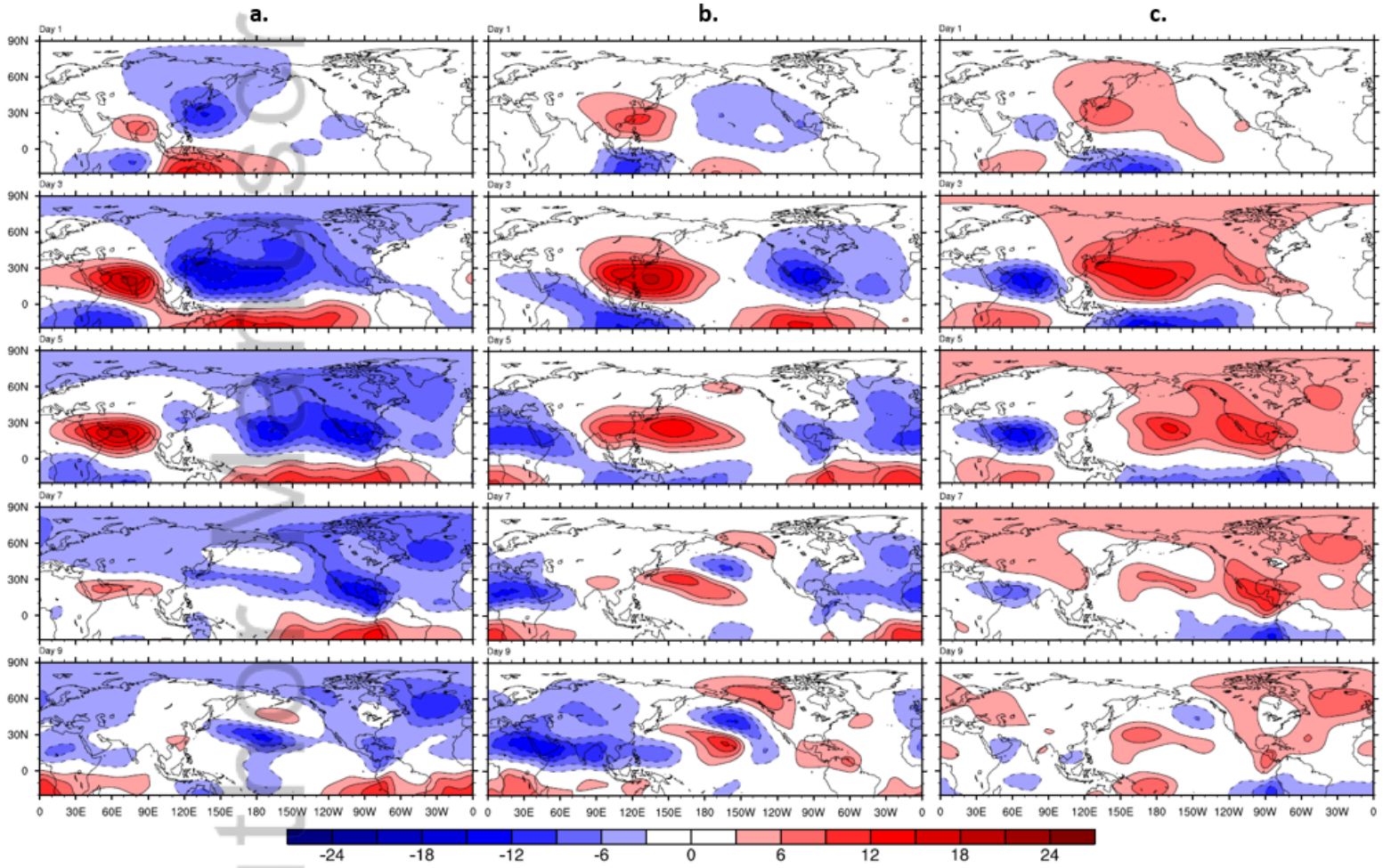

Lukens_et_al_QJRMS_Revised_Figure10.tif

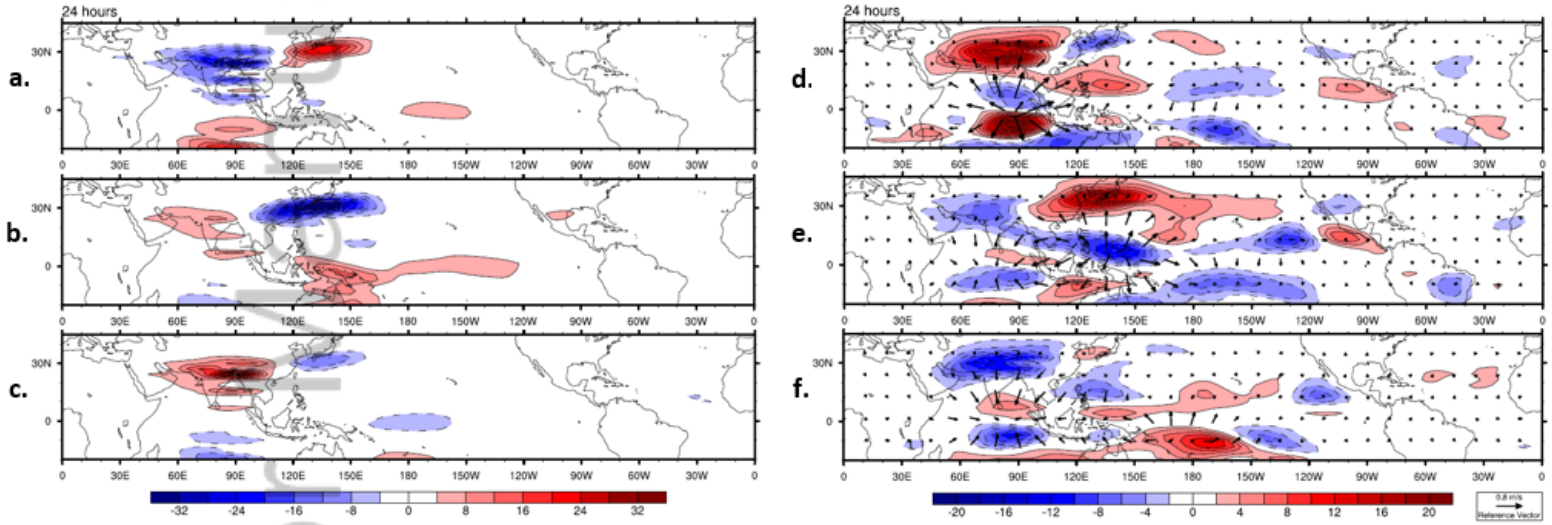

Lukens_et_al_QJRMS_Revised_Figure11.tif

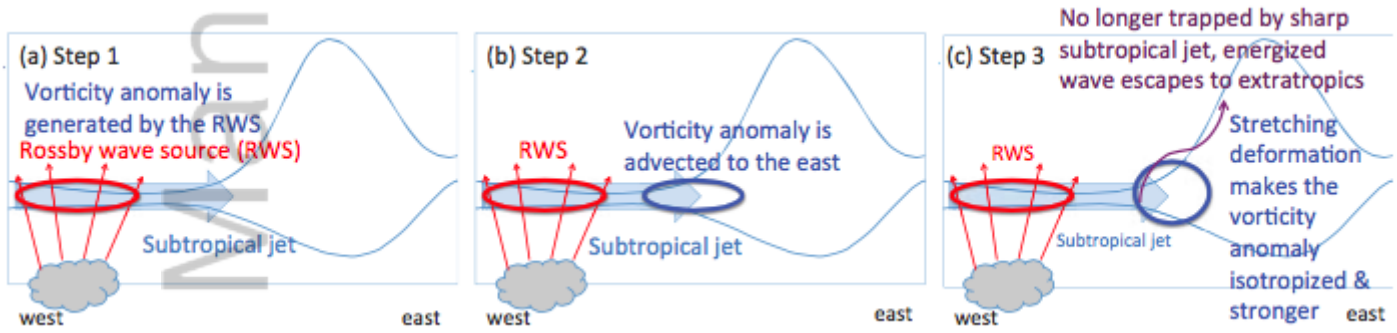

Lukens_et_al_QJRMS_Revised_Figure12.tif